Dalton Transactions

Accepted Manuscript

This is an *Accepted Manuscript*, which has been through the Royal Society of Chemistry peer review process and has been accepted for publication.

Accepted Manuscripts are published online shortly after acceptance, before technical editing, formatting and proof reading. Using this free service, authors can make their results available to the community, in citable form, before we publish the edited article. We will replace this *Accepted Manuscript* with the edited and formatted *Advance Article* as soon as it is available.

You can find more information about *Accepted Manuscripts* in the Information for Authors.

Please note that technical editing may introduce minor changes to the text and/or graphics, which may alter content. The journal's standard Terms & Conditions and the Ethical guidelines still apply. In no event shall the Royal Society of Chemistry be held responsible for any errors or omissions in this *Accepted Manuscript* or any consequences arising from the use of any information it contains.

ROYAL SOCIETY OF CHEMISTRY

www.rsc.org/dalton

RSCPublishing

ARTICLE

Synthesis and Characterization of a Family of M^{2+} Complexes Supported by a Trianionic ONO^{3-} Pincer-type Ligand: Towards the Stabilization of High-Spin Square-Planar Complexes

Cite this: DOI: 10.1039/x0xx00000x

Received ooth January 2012,
Accepted ooth January 2012

DOI: 10.1039/x0xx00000x

www.rsc.org/

M. E. Pascualini,[a] S. A. Stoian,[b*] A. Ozarowski,[b] N. V. Di Russo,[a] A. E. Thuijs,[a] K. A. Abboud,[a] G. Christou[a] and A. S. Veige[a*]

High-spin square-planar molecular compounds are rare. In an effort to access this unique combination of geometry and spin state, we report the synthesis of a series of M(II) compounds stabilized by a trianionic pincer-type ligand, highlighting the formation of a high-spin square-planar Co(II) complex. Low-temperature, variable-frequency EPR measurements reveal that the ground electronic state of the Co(II) analogue is a highly anisotropic Kramers doublet (effective g values 7.35, 2.51, 1.48). This doublet can be identified with the lowest doublet of a quartet, S = 3/2 spin state that exhibits a very large ZFS, D ¤ 50 cm^{-1}. The observation of an effective g value considerably greater than the largest spin-only value 6, demonstrates that the orbital angular moment is essentially unquenched along one spatial direction. Density Functional Theory (DFT) and time-dependent DFT calculations reveal the electronic configurations of the ground and excited orbital states. A qualitative crystal field description of the g_{eff} tensor shows that it originate from the spin-orbit coupling acting on states obtained through the transfer of a β electron from the doubly occupied *xy* to the singly-occupied {*xz*/*yz*} orbitals.

Despite decades of research on the interplay between molecular geometry and electronic structure within first-row transition metal complexes, efforts to exert control over these properties continue unabated.[1-4] In particular, four-coordinate complexes mainly manifest in two different geometries that coincide with two common spin states: tetrahedral complexes favor high-spin states and square-planar compounds have a marked preference for low-spin configurations.[5-11] Given the correct combination of ligands and choice of metal ion, the energetic difference between two different geometries and spin states can be extraordinarily narrow.[12] One compelling example comes from the four-coordinate Co(II) complex $[Co(Bc^{tBu})_2]$ (Bc^{tBu} = bis(3-*tert*-butylimidazol-2-ylidene)borate). Crystals of this compound contain low-spin S = 1/2 square-planar and high-spin S = 3/2 tetrahedral isomers in the asymmetric unit.[13] Another example that emphasizes the close relationship between geometry and spin state involves the bis-[N,N´-bis(2-biphenyl)-N-oxidoformamidinate] cobalt(II) complex that crystallizes as a green low-spin S = 1/2 square-planar compound or an orange high-spin S = 3/2 tetrahedral complex depending on crystallization conditions.[14]

Taking a close look at the d-orbital splitting caused by the ligand donors disposed in these geometries allows a better understanding of this phenomenon. Tetrahedral geometries break the d-manifold into two groups of degenerate orbitals, which are separated by a fairly small energy gap, allowing easy access to high-spin electronic configurations. In contrast, square-planar complexes present a very destabilized $d_{x^2-y^2}$ orbital resulting in a large energy gap rendering low-spin electronic configurations. As a consequence, high-spin square-planar metal complexes with d-counts greater than four are rare. Only a handful of examples appear in the literature, and most of them contain either macrocyclic or sterically demanding ligands, suggesting that the square-planar geometry is not exclusively driven by electronic factors.[15-20] Remarkably, Klüfers, in 2011 prepared the first electronically-driven square-planar high-spin Fe(II) molecular compound featuring a FeO_4 core.[21] Doerrer and co-workers recently reported a bidentate fluorinated alkoxide ligand capable of stabilizing only the second Fe(II), and the first Co(II) complexes exhibiting a square-planar geometry and high-spin state.[22] Holland illustrated a set of conditions to promote high-spin square-planar molecular compounds: (1) charge from anionic ligands to reduce the metal acidity and prevent coordination from additional ligands, (2) alkali metal counterions to stabilize the negative charge, (3) strong π-donor ligands to destabilize the

Dalton Transactions Accepted Manuscript

sterically preferred tetrahedral geometry, and most importantly, (4) weak σ-donating ligands to minimize the anti-bonding character of the $d_{x^2-y^2}$ orbital.[23]

Our group recently reported the trianionic pincer-type ligand 2,2'-(azanediylbis(2,1-phenylene))bis(1,1,1,3,3,3-hexafluoropropan-2-ol) ([CF_3-ONO]H_3; **1**) and its coordination to W(VI),[24-27] Ta(V),[28] Hf(IV),[29] Ti(IV),[29] Fe(III),[30] and Fe(II)[31] metal centers. Ligand **1** contains all the prerequisites described by Holland. Indeed, the ligand was successful in stabilizing the high-spin square-planar Fe(II) complex {[CF_3-ONO]FeCl}{Li(Sv)$_2$}$_2$ (**2**; Sv = tetrahydrofuran (THF), Et_2O). Complex **2** features a FeO_2NCl core, thus deviating from the homoleptic FeO_4 core. More importantly, for the first time, a frozen solution Mössbauer experiment provides clear evidence that **2** retains its uncommon geometry and spin state in solution, and therefore, is not the consequence of packing forces.[31] In this work we probe the capacity of the ONO^{3-} ligand to stabilize other first row transition metal ions as high-spin square planar complexes. Achieving this goal, we now report the synthesis and characterization of a rare high-spin square-planar Co(II) complex. Included is a rational explanation for why Mn(II) is unlikely to adopt this peculiar geometry and spin-state.

Treating a DME solution of proligand **1** with 3 equiv of lithium hexamethyldisilazide ($LiN(SiMe_3)_2$) produces the trilithio salt [CF_3-ONO]Li_3 in situ.[31] Adding the [CF_3-ONO]Li_3 solution to 1.2 equiv of a pink suspension of $MnCl_2$ in DME, and stirring the reaction mixture for 2 h produces a color change from pink to brown. Removing all volatiles under vacuum generates a brown oil that turns into a bright yellow powder after triturating with pentane several times. Dissolving this powder in Et_2O, and removing all the inorganic salts by filtering through a Celite™ pad produces an analytically pure bright yellow powder in 86% yield (Scheme 1). Cooling a concentrated Et_2O solution of **3** to -35 °C yields yellow crystals suitable for X-ray analysis.

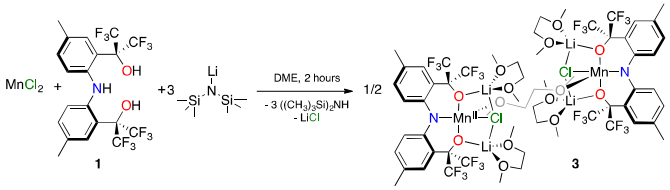

Scheme 1. Synthesis of **3**.

Depicted in Fig. 1 is the molecular structure of **3**. Table 1 lists pertinent metric parameters. Complex **3**, unlike the square-planar Fe(II) analogue, contains a DME ligand that acts as a bridge between the two otherwise square-planar fragments. The dimer resides on an inversion center located in the middle of the bridging DME and contains two Mn(II) atoms in a slightly distorted square-pyramidal geometry with an Addison parameter[32] τ of 0.134. Complex **3** presents a very long Mn1-Cl1 bond (2.5231(5) Å), due to the strong *trans* influence exerted by the amido N-atom from the pincer (Mn1-N1 = 2.0610(13) Å), and the electrostatic attraction caused by the neighbouring Li^+ counter cations. The Mn1-O1 and Mn1-O2 bond lengths are 2.0485(11) Å and 2.0639(11) Å, respectively, and they are more than 0.1 Å shorter than the Mn1-O7 bond distance of 2.1812(12) Å.

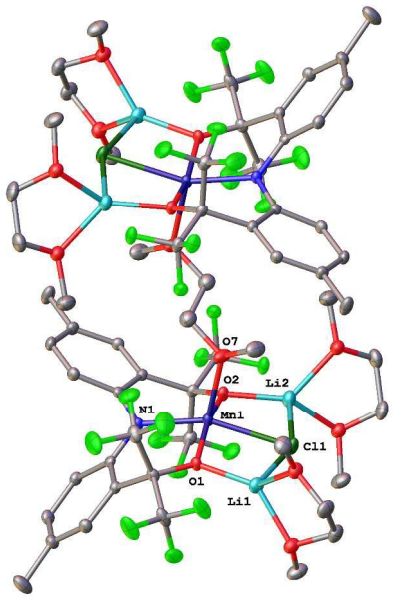

Fig. 1. Molecular structure of **3**. Ellipsoids drawn at 50% probability level. Hydrogen atoms are omitted for clarity.

One interesting question arises from the molecular geometry of **3**. When compared with its Fe(II) analogue, **3** possesses an extra donor ligand in the apical position generating a square-pyramidal geometry. By examining the molecular orbital diagram of **3** (Fig. 2), it is easy to understand the difference in coordination number. Bringing together a Mn(II) square-planar fragment and a σ-donating ligand in the apical position produces the formation of a bonding ligand-based and an antibonding metal-based molecular orbital combination with the Mn d_{z^2} orbital. Since two electrons reside in the bonding orbital, and only one electron in the antibonding orbital, a ligand field stabilization energy (LFSE) calculation dictates that the five-coordinate complex is more stable. In contrast, since Fe(II), Co(II), and Ni(II) analogues possess a doubly-occupied d_{z^2} orbital,[31] the coordination of a fifth ligand in the apical position does not result in any electronic stabilization. Indeed, the Fe(II) complex **2** is square-planar and high-spin[31] and preparation of the Co(II) analogue as a square-planar high-spin complex would mark only the second occurrence of such a species.

Dalton Transactions Accepted Manuscript

This journal is © The Royal Society of Chemistry 2012

RSCPublishing

ARTICLE

Table 1. Metric parameters derived from the molecular structures of compounds **2-5**.

Compound	Metal	Geometry	τ4	M-N1	M-Cl1	M-O1	M-O2	M-O7	Reference
3	Mn	Square-pyramidal	-	2.0610(13)	2.5231(5)	2.0485(11)	2.0639(11)	2.1812(12)	This work
2	Fe	Square-planar	0.071	1.9677(15)	2.3757(10)	1.9743(14)	1.9737(14)	-	30
4	Co	Square-planar	0.323	1.9154(16)	2.3855(6)	1.9291(13)	1.9291(13)	-	This work
5	Ni	Square-planar	0.059	1.8279(24)	2.2743(9)	1.8530(21)	1.8490(21)	-	This work

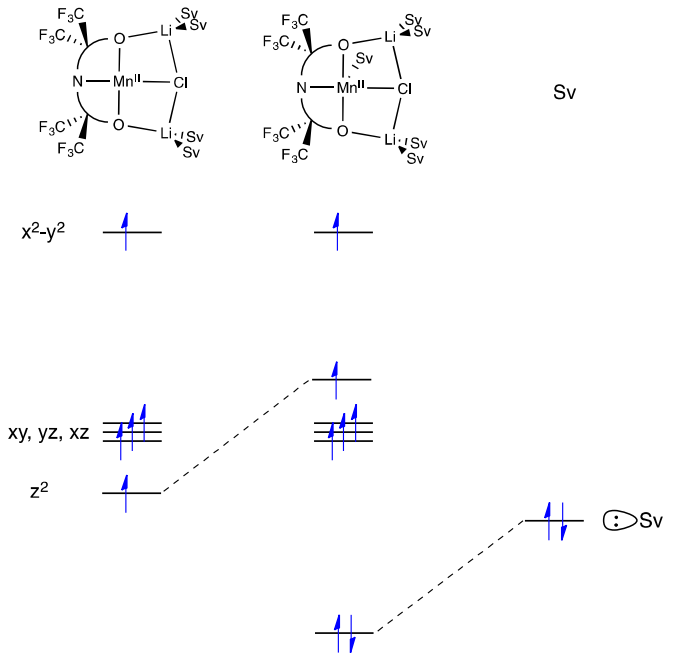

Fig. 2 Molecular orbital diagram of **3** derived from a fragment approach.

The electronic structure of **3** was established on the basis of the high-frequency EPR spectra recorded for frequencies ranging from 104 to 406 GHz at temperatures between 1.7 and 20 K. These spectra exhibit a prominent, derivative-type resonance that is centred at g ≈ 2.0 and is flanked on both sides by several less intense satellite peaks (Fig 3). Although **3** is a dimer the significant length of the bridging DME ligand suggests that the local Mn(II) sites are magnetically isolated and that the superexchange interactions between the two local sites are null. Consequently, we have analysed the HFEPR spectra of **3** in the framework of the spin-Hamiltonian described by eq 1 for which S = 5/2. Our analysis demonstrates that these spectra can be understood only by considering two very similar species with a 1:1 relative ratio.

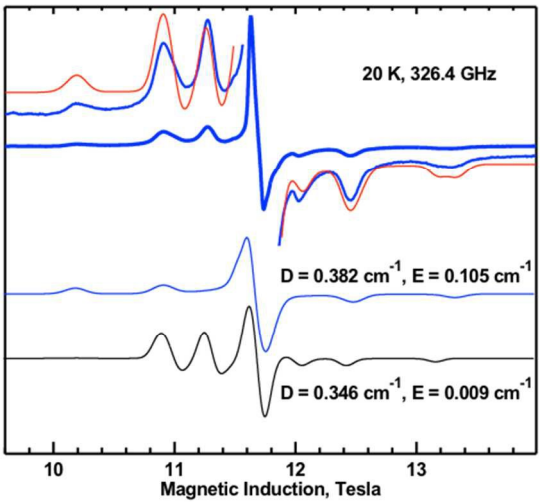

Fig. 3 The thick blue line in the upper spectrum represents the experimental high-field EPR spectrum for **3** at 20 K and 326.4 GHz. The red line is a combination of the two simulated spectra on the bottom and it is superimposed to a magnified portion of the experimental data also in blue.

This observation suggests that there are minor structural differences between the two subunits of the dimer which lead to a distinct environment for the two Mn(II) sites. Although the crystallographic investigation of **3** reveals the presence of an inversion center, considering the low energetic difference between the observed parameters ($\Delta D = 0.04$ cm^{-1}) the presence of two distinct EPR spectra originates from disorder of the two molecular halves that is below the limit of detection of our X-ray diffraction method. Finally, the sextet ground spin state of the two Mn(II) ions manifest a relatively small zero field splitting (ZFS) described by D ≈ 0.36(2) cm^{-1} and intrinsic g values that are very close to that of the free electron, g ≈ 2.01(1). These values are indicative of an isolated singlet ^{6}A orbital state and are in agreement with the expected properties of ions with high-spin, d^5 configurations.

$$\hat{H} = D\left[\hat{S}_z^2 - \frac{1}{3}S(S+1) + \frac{E}{D}\left(\hat{S}_x^2 - \hat{S}_y^2\right)\right] + \beta\vec{\mathbf{B}}\cdot\tilde{\mathbf{g}}\cdot\hat{\mathbf{S}} \qquad \text{Eq. 1}$$

Dalton Transactions Accepted Manuscript

The synthesis of the Co(II) analogue **4** follows a similar procedure to its Mn(II) counterpart. Three equivalents of base are added to **1**, and this mixture is slowly transferred to a sky blue $CoCl_2$ suspension. The identity of the solvent produces dramatically different results: using THF or Et_2O results in intractable mixtures as a consequence of poor $CoCl_2$ solubility. However, stirring a DME mixture for 2 h yields a pronounced color change from sky blue to red-brown. After removing all volatiles under vacuum and inorganic salts by dissolving the compound in Et_2O and filtering through a Celite™ pad, an analytically pure orange microcrystalline powder is obtained in 47% yield (Scheme 2). Cooling a concentrated Et_2O solution of **4** to -35 °C yields red crystals suitable for X-ray interrogation.

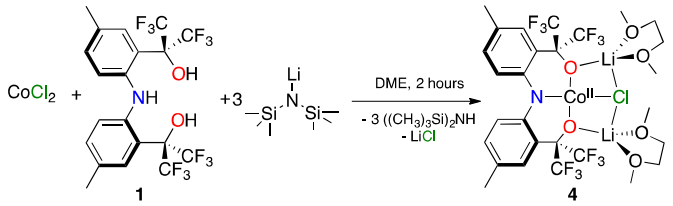

Scheme 2 Synthesis of **4**.

Fig. 4 depicts the molecular structure of **4**, and Table 1 lists pertinent metric parameters. A distorted square-plane best describes the coordination geometry of complex **4** with the $[CF_3\text{-}ONO]^{3-}$ pincer-type ligand and a Cl occupying the square-base (τ_4 = 0.323).[33] The Co1-N1 bond (1.9154(16) Å) is 0.4701(17) Å shorter than the Co1-Cl1 bond (2.3855(6) Å) as a consequence of the strong *trans* influence of the amido N-atom and the electrostatic attraction from the Li^+ counterions. The Co1-O1 and Co1-O2 bonds located *trans* to each other are statistically identical (1.9291(13) Å). These Co-O bond lengths compare well with those reported for the only other high-spin square-planar Co(II) complex (1.9516(12) Å and 1.9510(12) Å).[22]

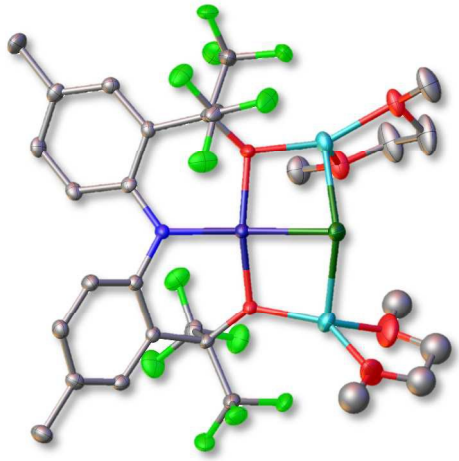

Fig. 4 Molecular structure of **4**. Ellipsoids drawn at 50% probability level. Hydrogen atoms are omitted for clarity.

The EPR spectra recorded for a powder sample of **4** at microwave frequencies from 50 to 410 GHz and temperatures from 3.0 to 20.0 K exhibit a rhombic signal that is characterized by a highly anisotropic set of effective *g* values (Fig. 5). This signal originates from the ground Kramers doublet of a S = 3/2 spin manifold and was analyzed in the framework of the spin-Hamiltonian described by Eq. 1 where S = 3/2. Interestingly, the low-field resonance is defined by g_{eff} = 7.35; a value that is considerably larger than 6. In the absence of spin-orbit coupling ($g_{x,y,z} \sim 2.00$), the latter value corresponds to the maximum g_{eff} that can be observed for a quartet spin state *i.e.* $g_{eff}(\max) = 3\ g_i$ where i = x, y, z. Consequently, this observation demonstrates that at least one of the three components of the intrinsic *g* tensor is considerably larger than that of the free electron (g_e = 2.0023) such that $g_i \geq 2.45$. This finding is in turn indicative of a sizable, spin-orbit mediated mixing of a low-lying orbital state into the ground state of **4**.

The effective *g*-values describing the field-dependent behaviour of the two Kramers doublets are not only dependent on the intrinsic *g* tensor but also on the details of the zero-field splitting of the S = 3/2 state. Inspection of Figure S16 shows that in the low Zeeman field limit the effective *g*-values of a particular doublet are essentially independent of the axial ZFS parameter *D* and are strongly correlated with the rhombic ZFS parameter *E*/*D*.[34-35] Thus, the maximum *g* value ($g_{eff,\ z} \sim 6$), is associated with the $|S, m_s\rangle = |3/2, \pm 3/2\rangle$ doublet and is observed at $E/D \sim 0$. Furthermore, under these conditions, this doublet is expected to exhibit uniaxial magnetic properties that is, $g_{x,y} \sim 0$.[36] For **4**, the ground Kramers doublet exhibits a EPR signal for which the two lowest effective *g* values are considerably larger than zero. This in turn, indicates the presence for this complex of a large *E*/*D* value such that $E/D \geq 0.25$. It is important to note that according to Figure S16 as *E*/*D* increases in value, the similarity between the magnetic properties of the two doublets intensifies such that at $E/D \sim 0.33$ they are essentially indistinguishable from one another and that the sign of *D* is undetermined. Consequently, owing to the large *E*/*D* value, based only on the effective *g* values of the ground doublet we cannot assign a sign to *D*.

Typically, the ZFS parameter *D* that accounts for the energy separation of the two doublets might be determined using EPR either by observing resonances that arise from inter-doublet transitions or by analysing the temperature dependence of the signals associated with the two Kramers doublets. Unfortunately, increasing the temperature did not allow for the detection of a signal associated with the excited doublet and increasing the microwave frequency to 410 GHz and the applied field to 14 T did not lead to the observation of a direct inter-Kramers transition. Although *D* cannot be established from these observations, it is possible to determine that $|D| \geq 20$ cm^{-1}. The presence of a large $|D|$ is further corroborated by the frequency dependence of the observed resonances. In particular, the curvatures of the frequency dependence of the x and y resonances result from the interplay of $|\vec{\mathbf{B}}|$, the applied field, and $|D|$. Thus, the $\mu_B g_i B_i \hat{S}_i$ (where i = x, y) components of the Zeeman operator induce a mixing of the excited doublet

Dalton Transactions Accepted Manuscript

This journal is © The Royal Society of Chemistry 2012

levels into those of the ground doublet. However, the magnitude of this field-induced mixing is determined by the energy separation between the two doublets and consequently the slopes of the frequency dependence of the x and y resonances are proportional to the $|\mu_B B/D|$. The frequency dependencies of the resonant field of all three resonances observed for **4** are essentially linear which indicates that $|D| >> |\mu_B B|$ and allows us to establish that $|D| \geq 50$ cm^{-1} (Fig. 5, bottom).

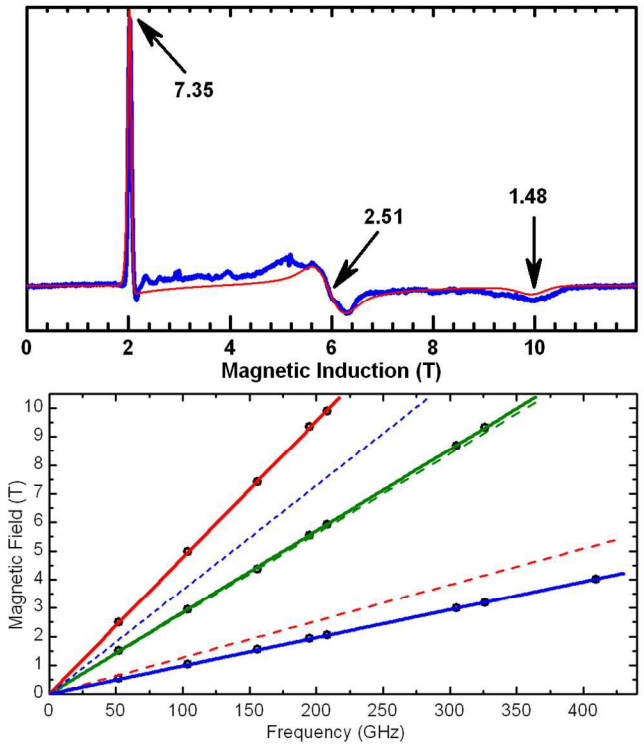

Fig. 5 *Top*: High-field EPR spectrum recorded for 4 at 208 GHz and 5 K. The solid red trace is a simulation obtained for a S = 3/2 spin system using D = 175 cm^{-1}, E/D = 0.33, g_x = 2.528, g_y = 2.661 and g_z = 2.061. We note that these values are not unique, that from this data only a low limit for D can be established (D ¤ 50 cm^{-1}), and that the same effective g values can be obtained by trading $g_{x,y,z}$ values for a different E/D, see text. The arrows highlight the effective g-values of the observed resonances. *Bottom*: Black dots mark the field- and frequency-dependence of the observed resonances. The solid (ground doublet) and dotted (excited doublet) lines account for the predicted dependencies derived from the parameters listed above. The red, blue and green colors mark the z, y and x molecular orientations.

To establish the electronic structure of **4** and to rationalize the observed spectroscopic parameters a series of Density Functional Theory (DFT) and crystal field (CF) calculations were performed. The DFT calculations of **4** were carried at the B3LYP/6-311G level of theory and used the structural models shown in Figure S14 of ESI. The geometry optimizations yielded predicted bond lengths and angles that are in good agreement with the X-ray structure see Table S17. Furthermore, these calculations indicate that the ground state exhibits a S = 3/2 spin value and that it is found about 3200 cm^{-1} below the lowest S = 1/2 state. Inspection of the gross orbital population reveals that this state is best described as $|(xy)^2(z^2)^2(xy)^+(xz)^+(x^2\text{-}y^2)^+|$, see Table S19. The ground-state character of this state was established on the basis of time-dependent (TD) DFT calculations which yielded only positive excitation energies. The lowest excitations correspond to d-d transitions and are listed in Table S18. The ground electronic configuration belongs to the ^{4}F ground term of the free Co^{2+} ion. The stabilization of this particular state is a consequence of the nonbonding character and thus of the lower energies of the $\{xy, z^2\}$ orbitals and of the minimal interelectronic repulsions between the 3d electrons expected for this configuration.

Fig 6 presents the excitation energies of the 3d orbital-based β electrons as predicted by TD DFT. The energies of these excitations were expressed in terms of 3d orbital energies, $\varepsilon(i)$, and of the Racah parameter B, see Table S20. The latter parameter is a measure of the Coulomb repulsions between the 3d electrons. The numerical values of the 3d orbital energies and of the parameter B are listed in Table S21 and were obtained by minimizing the difference between the DFT-predicted values and those obtained using the theoretical expression listed in Table S20. Interestingly, the resulting set of $\varepsilon(i)$ values leads to a crystal field splitting pattern that is very similar to that observed for the iron(II) based analogue, complex **2**. The d-d transitions of a Fe^{2+} ion with a ^{5}D ground state originating from a d^6 electronic configuration, are not dependent on the Racah parameters and can be directly identified with the crystal field splitting of the 3d orbitals. The B value predicted for **4,** B = 550 – 680 cm^{-1}, although smaller than that of the free ion, B ◊ 1000 cm^{-1}, is considerably higher than the DFT-based value predicted for the pre-eminently covalent compound $[Co(CN)_6]^{3-}$, B = 390 - 460 cm^{-1}, and implies that **4** exhibits an increased ionic character.[37] Inspection of the crystal field splitting pattern of the 3d orbitals shown in Fig 6 suggests that the two lowest excited orbital states correspond to the $\{xy \rightarrow xz\}$ and $\{xy \rightarrow yz\}$ configurations obtained through the transfer of a β electron from the doubly occupied xy orbital to the xz and respectively, the yz singly occupied orbitals. However, analysis of the TD DFT results reveals that the lowest four excitations are expressed as a linear combination of single electron excitations involving the $\{xy, z^2\} \rightarrow \{yz, xz\}$ pairs of orbitals. This in turn indicates that the four lowest excited orbital states are multi-determinantal in nature and are expressed as a linear combination of individual configurations derived from the promotion of a β electron to and from either one of xz/yz and z^2/xy orbitals. This observation can be easily understood when considering that the numerical values of the individual one electron excitations involving this particular set of orbitals are nearly identical in spite of the large difference in the contributions of the interelectronic repulsion to their total (6B), see Table S20. Comparison of the two lowest orbital excited states predicted by the two lowest TD DFT excitations with the individual states of the ^{4}F term of the free Co^{2+} ion suggests that, similar to the ground state, the two lowest excited states have a nearly pure ^{4}F character, see Table S22. Interestingly, the matrix elements of the $\hat{L}_\xi$ operators (where $\xi = x, y, z$) involving the $|(xy)^2(z^2)^2(xy)^+(xz)^+(x^2\text{-}y^2)^+|$ ground state (GS) and the first two excited states derived from the analysis of the TD DFT results are identical to those

Dalton Transactions Accepted Manuscript

involving GS and the $\{xy \rightarrow xz\}$ and $\{xy \rightarrow yz\}$ configurations, see Table S23. This observation demonstrates that describing the magnetic properties of **4** by considering the spin-orbit coupling of the ground state with the DFT-based or the CF-derived excited states is in fact equivalent. In the following, for simplicity's sake we will use the CF description.

Analysis of the HFEPR spectra recorded for **4** demonstrate that its ground spin state exhibits a large ZFS ($|D| \approx 50$ cm^{-1}) and a highly anisotropic ground Kramers doublet. These observations reveal the presence for this complex of a large unquenched orbital momentum. The unquenching of the orbital momentum is a consequence of a strong spin-orbit mediated interaction between the ground orbital state and one or more low-lying excited orbital states. Inspection of Fig 6, suggests that the unquenching of the orbital momentum involves either one or both of the two low-lying orbital states corresponding to the $\{xy \rightarrow yz\}$ and $\{xy \rightarrow xz\}$ configurations. For the case where the three lowest orbital states are degenerate i.e., triplet orbital ground state, under the action of the spin-orbit coupling, $\hat{H}_{SO} = \lambda \hat{\mathbf{L}} \cdot \hat{\mathbf{S}}$, the twelve spin-orbit states split into a doublet, a quartet and a sextet. These states can be described using fictitious angular momenta J' = 1/2, 3/2 and 5/2 and the ground state is given by the J' = 1/2 doublet. The ground doublet is isotropic, is characterized by a $g_{eff} \approx 4$, and is found approximately $|3\zeta/2| \approx 270$ cm^{-1} below the quartet state assuming the free ion value of $\zeta \approx -180$ cm^{-1}.[38] This situation is analogous to that expected for Co(II) ions placed in a highly symmetric cubic environment.

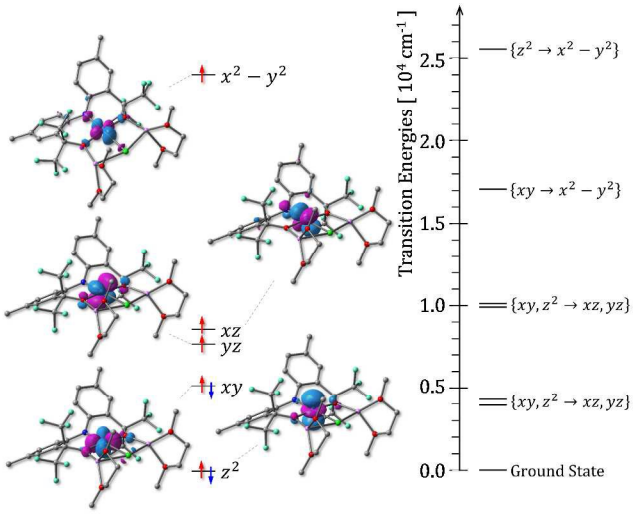

Fig. 6 Relative splitting of the d orbital set (*left*) as determined from the analysis of the TD-DFT excitations (*right*). Analysis of the four lowest excitations suggests that the four lowest excited orbital states are multi-determinantal in nature and are expressed as a linear combination of individual configurations derived from the promotion of a β electron to and from either one of *xz*/*yz* and z^2/*xy* orbitals.

If instead only two orbital states are degenerate and the other is far removed in energy i.e. $E(GS) \approx E(\{xy \rightarrow xz\}) \approx 0 << E(\{xy \rightarrow yz\})$ or $E(GS) \approx E(\{xy \rightarrow yz\}) \approx 0 << E(\{xy \rightarrow xz\})$, the spin-orbit interactions induces the lowest eight spin-orbit states to split up into a series of four equidistant doublets that are separated from one another by an energy difference equal to $|\zeta|$. The magnetic properties of these doublets can be easily determined considering the orbital wavefunctions that diagonalize the spin-orbit coupling operator. To illustrate this point consider the case where the GS and $\{xy \rightarrow yz\}$ configurations are degenerate. Under these conditions the two orbital levels exhibit maximal mixing and the *xy* β HOMO orbital can be replaced with a complex orbital of the form $|\pm\rangle = (xy \pm i\, yz)/\sqrt{2}$ such that the expectation values of the $\hat{L}_\xi$ operators are $\langle\pm|\hat{L}_y|\pm\rangle = \mp 1$ and $\langle\pm|\hat{L}_x|\pm\rangle = \langle\pm|\hat{L}_z|\pm\rangle = 0$.[39] Provided that the spin is quantized along *y* the spin-orbit functions of the $|\pm, \mathrm{M}_S\rangle \equiv |\pm\rangle \otimes |S = 3/2, \mathrm{M}_S\rangle$ form are eigenvectors of the spin-orbit coupling operator $\hat{\mathrm{H}}_{SO} = \lambda \hat{\mathrm{L}}_y \hat{\mathrm{S}}_y$. The effective g values of these doublets can be determined by evaluating the matrix elements of the Zeeman operator, $\hat{\mathrm{H}}_Z = \beta(\hat{\mathbf{L}} + 2\hat{\mathbf{S}})\vec{\mathbf{B}}$, and comparing them with those obtained for a fictitious S' = 1/2 spin, $\hat{\mathrm{H}}_Z = \beta \hat{\mathbf{S}}' \cdot \tilde{\boldsymbol{g}} \cdot \vec{\mathbf{B}}$, see Fig S15. Thus we find that the ground doublet corresponds to the $|\pm, \mp 3/2\rangle$ states which, for the degenerate case yield an effective set of g values such that (g_x = 0, g_y = 8, g_z = 0) where [g_y = 2(1+3)]. The essential difference between the case discussed above and that for which the GS and $\{xy \rightarrow xz\}$ configurations are degenerate is given by a reorientation of the easy axis of magnetization from y to the x that is, (g_x = 8, g_y = 0, g_z = 0).[40] The removal of the orbital degeneracy leads to a lowering of the large g_{eff} = 8. Additionally, interaction of the GS with other excited orbital states leads to non-zero g_{eff} values.[41] Our estimates of the effective g-values from the full diagonalization of the spin-orbit coupling operator matrix spanning the three lowest orbital states suggest that the first orbital state is found $\approx |\zeta| \approx 150$ - 180 cm^{-1}, and the second $\approx 6|\zeta| \approx 1000$ cm^{-1} above the GS, see Fig S15. Although these values are nearly one order of magnitude lower than those predicted by TD DFT this observation is not surprising when considering the errors associated with this method.[42]

The synthesis of the Ni(II) complex **5** is analogous to that of compounds **3** and **4**. Employing $NiCl_2$•DME improves the solubility of the metal substrate. Adding the in situ generated $[CF_3\text{-ONO}]Li_3$ salt to a yellow DME suspension of $NiCl_2$•DME and stirring this mixture for 2 h produces a green solution. After removing all volatiles under vacuum and inorganic salts by filtrating an Et_2O solution through a Celite™ pad, an analytically pure green powder is produced in 57% yield (Scheme 3). Unlike complexes **2**, **3**, and **4**, sharp signals in the ^{1}H and ^{19}F NMR spectra of compound **5** in C_6D_6 indicates it is diamagnetic. The ^{19}F NMR spectrum indicates **5** is C_2-symmetric with two quartets resonating at -72.92 and -76.49 ppm. Accordingly, the ^{1}H NMR spectrum exhibits only three aromatic resonances at 7.55, 7.49, and 6.81 ppm, and a singlet at 2.14 ppm (-CH_3) that correspond to the ONO ligand. Cooling a concentrated Et_2O solution of **5** to -35 °C yields green crystals suitable for X-ray analysis.

Dalton Transactions Accepted Manuscript

This journal is © The Royal Society of Chemistry 2012

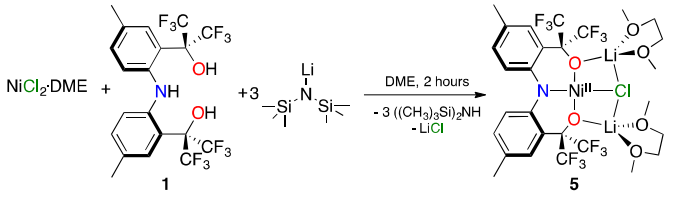

Scheme 3 Synthesis of **5**.

Fig. 7 depicts the solid-state structure of **5**, and Table 1 lists pertinent metric parameters. Consistent with the solution assignment, **5** is C_2-symmetric in the solid state. The asymmetric unit exhibits two chemically equivalent but crystallographically independent Ni complexes. All the bond distances between the independent complexes vary by 0.0094(9) Å or less. The Ni(II) center adopts an almost perfect square-planar geometry, reflected by its average τ_4 value[33] of 0.059. The fact that the low-spin Ni(II) complex presents the most perfect square-planar geometry of all the series highlights the relationship between geometry and electronic configurations. In fact, the ligand backbone twists to fulfil the electronic requirements imposed by the square-planar geometry. The short Ni1-N1 average bond length of 1.8279(24) Å reflects the smaller size of the low-spin Ni(II) cation. *Trans* to the Ni1-N1 bond, the average Ni1-Cl1 bond is much longer (2.2743(9) Å). Finally, the Ni1-O1 and Ni1-O2 average bond lengths are 1.8530(21) Å and 1.8490(21) Å, respectively.

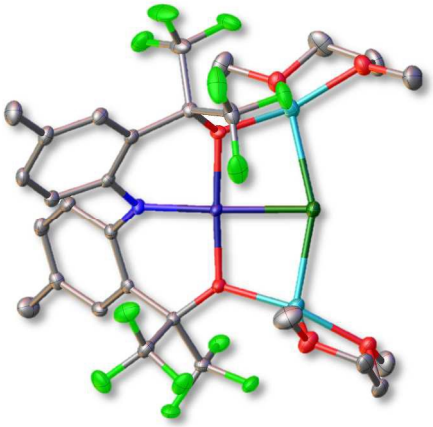

Fig. 7 Molecular structure of **5**. Ellipsoids drawn at 50% probability level. Hydrogen atoms are omitted for clarity.

The electrochemical properties of complexes **3-5** were investigated in acetonitrile/0.1 M Bu_4NPF_6 using a Pt mesh as a working electrode. Fig. 8 depicts the resulting cyclic voltammograms. All values in this work are reported vs ferrocene (Fc/Fc^+). The cyclic voltammograms of complexes **3-5** present reversible M(III)/M(II) couples with $E_{1/2}$ of 0.07 V, -0.56 V, and -0.33 V, respectively, highlighting the $[CF_3\text{-}ONO]^{3-}$ ligand's ability to stabilize high oxidation state metal complexes. Interestingly, the high-spin square-planar Co(II) complex $[Co(pin^F)_2]^{2-}$ (pin^F = dodecafluoropinacolate) features an irreversible oxidation process with an estimated $E_{1/2}$ at 0.09 V.[22, 43] In contrast, the cyclic voltammogram of **4** reveals a reversible Co(III)/Co(II) couple with $E_{1/2}$ at -0.56 V, which is comparable with the reduction potential of $[Co(NH_3)_6]^{3+}$ (-0.53 V).[44]

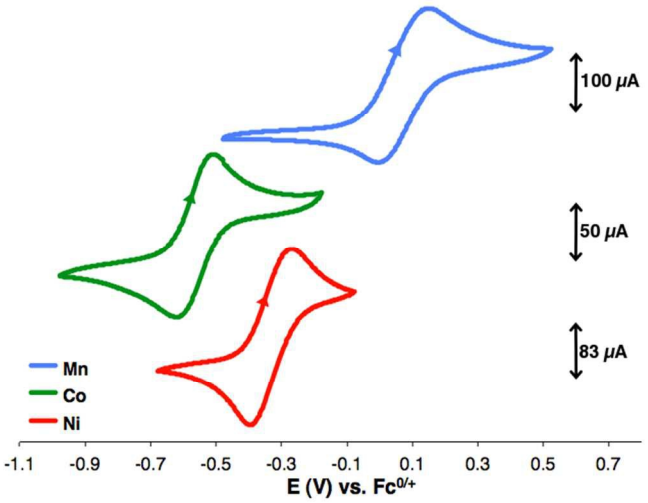

Fig. 8 Cyclic voltammograms of complexes **3-5** in acetonitrile using 0.1 M Bu_4NPF_6 as supporting electrolyte and a scan rate of 100 mV/s. Working electrode: Pt mesh. Reference electrode: Ag/AgCl. Auxiliary electrode: Pt wire.

Conclusions

This work presents the synthesis and characterization of a new M(II) series of first-row compounds stabilized by the trianionic $[CF_3\text{-}ONO]^{3-}$ pincer-type ligand. The pincer ligand provides two weakly σ-donating fluorinated alkoxides in the flanking arms and a strong π-donating amido N-atom in the central position providing a proper environment for stabilizing unique high-spin square-planar species. X-ray crystallography studies confirm the square-pyramidal structure of the Mn(II) compound, and the square-planar geometry of Fe(II), Co(II), and Ni(II) complexes. The Ni(II) analogue is diamagnetic and constitutes a hallmark example of low-spin d^8 Ni(II) compounds. The spectroscopic investigation of the Co(II) analogue revealed the presence of an unquenched orbital momentum rationalized on the basis of the spin-orbit interaction between the three lowest orbital states and consequently, we conclude that Co(II) square-planar complexes are good candidates for designing novel, 3d metal - based single molecule magnets. Finally, the Fe(II) and Co(II) complexes are examples of elusive high-spin square-planar species, where the Co(II) analogue is only the second example of a non-macrocyclic or sterically-driven molecular compound of this kind.

Acknowledgements

ASV acknowledges UF for providing funding for this research. This material is based upon work supported by the National Science Foundation CHE-1265993 (ASV) and DMR-1213030

Dalton Transactions Accepted Manuscript

(GC). KAA acknowledges the NSF (CHE-0821346) for the purchase of X-ray equipment. Computational resources were provided by the University of Florida High-Performance Computing Center. NVD is an HHMI International Student Research fellow. Part of this work was performed at the National High Magnetic Field Laboratory (NHMFL) which is supported by the NSF (DMR-1157490) and the State of Florida. SAS is an NHMFL Jack E. Crow postdoctoral fellow. This research was also supported in part by the NSF through TeraGrid resources provided by TACC under grant number TG-DMR100055.

Notes and references

[a] Department of Chemistry, Center for Catalysis, University of Florida, Gainesville, FL 32611 (USA). E-mail: veige@chem.ufl.edu
[b] National High Magnetic Field Laboratory, Florida State University, Tallahassee, FL 32310 (USA). E-mail: sebastian.stoian@magnet.fsu.edu

Electronic Supplementary Information (ESI) available: Detailed experimental conditions, elemental analysis, NMR spectroscopy, magnetic susceptibility data and fitting, HFEPR spectroscopy, and DFT calculations. CCDC reference numbers 1420980 (**4**), 1420981 (**3**), and 1420982 (**5**). For ESI and crystallographic data in CIF or other electronic format see DOI: 10.1039/b000000x/

1 F. A. Cotton, *Advanced Inorganic Chemistry*, Wiley, New York, 1999
2 P. L. Holland, *Acc. Chem. Res.*, 2008, **41**, 905-914.
3 R. Poli, *Chem. Rev.*, 1996, **96**, 2135-2204.
4 E. I. Solomon, K. M. Light, L. V. Liu, M. Srnec and S. D. Wong, *Acc. Chem. Res.*, 2013, **46**, 2725-2739.
5 E. J. Hawrelak, W. H. Bernskoetter, E. Lobkovsky, G. T. Yee, E. Bill and P. J. Chirik, *Inorg. Chem.*, 2005, **44**, 3103-3111.
6 S. P. Semproni, C. C. H. Atienza and P. J. Chirik, *Chem. Sci.*, 2014, **5**, 1956-1960.
7 S. C. Bart, E. J. Hawrelak, A. K. Schmisseur, E. Lobkovsky and P. J. Chirik, *Organometallics*, 2004, **23**, 237-246.
8 E. R. King and T. A. Betley, *J. Am. Chem. Soc.*, 2009, **131**, 14374-14380.
9 J. Zhang, W. Gao, X. Lang, Q. Wu, L. Zhang and Y. Mu, *Dalton Trans.*, 2012, **41**, 9639-9645.
10 G. Henkel, K. Greiwe and B. Krebs, *Angew. Chem. Int. Ed.*, 1985, **24**, 117-118.
11 A. Dolega, A. Jablonska, A. Pladzyk, L. Ponikiewski, W. Ferenc, J. Sarzynski and A. Herman, *Dalton Trans.*, 2014, **43**, 12766-12775.
12 C. A. Reed and F. Guiset, *J. Am. Chem. Soc.*, 1996, **118**, 3281-3282.
13 Y. Z. Liu, J. Wang, Y. Zhao, L. Chen, X. T. Chen and Z. L. Xue, *Dalton Trans.*, 2015, **44**, 908-911.
14 M. Cibian and G. S. Hanan, *Chem-Eur J*, 2015, **21**, 9474-9481.
15 V. Esposito, E. Solari, C. Floriani, N. Re, C. Rizzoli and A. Chiesi-Villa, *Inorg. Chem.*, 2000, **39**, 2604-2613.
16 C. A. Nijhuis, E. Jellema, T. J. J. Sciarone, A. Meetsma, P. H. M. Budzelaar and B. Hessen, *Eur. J. Inorg. Chem.*, 2005, **2005**, 2089-2099.
17 B. S. Kang, Z. N. Chen, Y. X. Tong, H. Q. Liu, H. R. Gao, B. M. Wu and T. C. W. Mak, *Polyhedron*, 1997, **16**, 1731-1737.
18 J. Jubb, D. Jacoby, C. Floriani, A. Chiesvilla and C. Rizzoli, *Inorg. Chem.*, 1992, **31**, 1306-1308.
19 D. Christodoulou, M. G. Kanatzidis and D. Coucouvanis, *Inorg. Chem.*, 1990, **29**, 191-201.
20 S. De Angelis, E. Solari, C. Floriani, A. Chiesi-Villa and C. Rizzoli, *J. Am. Chem. Soc.*, 1994, **116**, 5691-5701.
21 X. Wurzenberger, H. Piotrowski and P. Klüfers, *Angew. Chem. Int. Ed.*, 2011, **50**, 4974-4978.
22 S. A. Cantalupo, S. R. Fiedler, M. P. Shores, A. L. Rheingold and L. H. Doerrer, *Angew. Chem. Int. Ed.*, 2012, **51**, 1000-1005.
23 P. L. Holland, *Nat. Chem.*, 2011, **3**, 507-508.
24 M. E. O'Reilly, I. Ghiviriga, K. A. Abboud and A. S. Veige, *J. Am. Chem. Soc.*, 2012, **134**, 11185-11195.
25 M. E. O'Reilly, I. Ghiviriga, K. A. Abboud and A. S. Veige, *Dalton Trans.*, 2013, **42**, 3326-3336.
26 S. A. Gonsales, M. E. Pascualini, I. Ghiviriga, K. A. Abboud and A. S. Veige, *J. Am. Chem. Soc.*, 2015, **137**, 4840-4845.
27 S. A. Gonsales, M. E. Pascualini, I. Ghiviriga and A. S. Veige, *Chem. Commun.*, 2015, DOI: 10.1039/C1034SC02634A.
28 S. VenkatRamani, M. E. Pascualini, I. Ghiviriga, K. A. Abboud and A. S. Veige, *Polyhedron*, 2013, **64**, 377-387.
29 S. S. Nadif, J. Pedziwiatr, I. Ghiviriga, K. A. Abboud and A. S. Veige, *Organometallics*, 2015, **34**, 1107-1117.
30 M. E. Pascualini, N. V. Di Russo, P. A. Quintero, A. E. Thuijs, D. Pinkowicz, K. A. Abboud, K. R. Dunbar, G. Christou, M. W. Meisel and A. S. Veige, *Inorg. Chem.*, 2014, **53**, 13078-13088.
31 M. E. Pascualini, N. V. Di Russo, A. E. Thuijs, A. Ozarowski, S. A. Stoian, K. A. Abboud, G. Christou and A. S. Veige, *Chem. Sci.*, 2015, **6**, 608-612.
32 A. W. Addison, T. Nageswara Rao, J. Reedijk, J. van Rijn and G. C. Verschoor, *J. Chem. Soc., Dalton Trans.*, 1984, 1349-1356.
33 L. Yang, D. R. Powell and R. P. Houser, *Dalton Trans.*, 2007, 955-964.
34 J. R. Pilbrow, *J. Magn. Res.*, 1978, **31**, 479-490.
35 F. Lattanzi, *J. Physique Lett.*, 1982, **43**, 383-387.
36 R. Aasa and T. Vanngard, *J. Magn. Res.*, 1975, **19**, 308-315.
37 A. Atanasov, C. A. Daul and C. Rauzy, *Structure and Bonding*, 2004, **106**, 97-125.
38 A. Abragam and B. Bleaney, *Electron Paramagnetic Resonance of Transition Ions*, Dover Publications, Inc, New York, 1986 Chapter 7, p 403.
39 S. A. Stoian, Y. Yu, J. M. Smith, P. L. Holland, E. L. Bominaar and E. Münck, *Inorg Chem*, 2005, **44**, 4915-4922.
40 Based on the current set of experimental data we cannot determine whether the easy axis of magnetization is aligned with the OCoO or the NCoCl axis of the [CoO_2ClN] chromophore
41 H. Andres, E. L. Bominaar, J. M. Smith, N. A. Eckert, P. L. Holland and E. Münck, *J Am Chem Soc*, 2002, **124**, 3012-3025.
42 K. B. Wiberg, R. E. Stratmann and M. J. Frisch, *Chem Phys Lett*, 1998, **297**, 60-64.
43 L. Tahsini, S. E. Specht, J. S. Lum, J. J. M. Nelson, A. F. Long, J. A. Golen, A. L. Rheingold and L. H. Doerrer, *Inorg. Chem.*, 2013, **52**, 14050-14063.
44 A. J. Bard, R. Parsons and J. Jordan, *Standard potentials in aqueous solution*, M. Dekker, New York, 1985

Dalton Transactions Accepted Manuscript

 This journal is © The Royal Society of Chemistry 2012

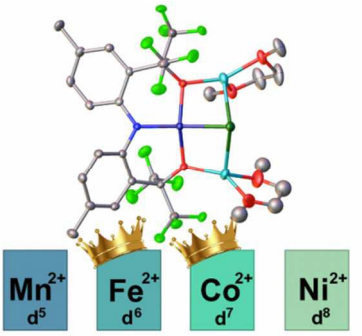

A trianionic pincer-type ligand stabilizes rare Fe(II) and Co(II) high spin, square-planar complexes.

Dalton Transactions Accepted Manuscript